Influence of Thermal Cycles on Current Sharing Temperature in ITER Toroidal Field Insert Coil Tests

Tomone Suwa, Takaaki Isono, Keiya Takebayashi, Yasuhiro Uno, Tsutomu Kawasaki, and Masaru Kawabe

***Abstract*—The ITER toroidal field (TF) conductors are cable-in-conduit conductors having Nb_3Sn strands. A TF insert coil (TFI) was fabricated, and its current sharing temperature (T_{cs}) was measured by using a uniform magnetic field and also applying hoop stress to simulate the actual operating conditions (68 kA in 11.8 T) of the ITER TF coils. The current sharing temperature (T_{cs}) of the TFI was degraded by warm-up and cool-down (WUCD) cycles that were performed after an initial 1000 electromagnetic loading cycles in its first test campaign. Current sharing temperature (T_{cs}) continued to degrade with subsequent WUCD cycles, which raised concerns that T_{cs} had decreased below the ITER requirement of 5.7 K. To further investigate this T_{cs} degradation by WUCD cycles, additional WUCD cycles were applied to the TFI (nine in total) and its T_{cs} was remeasured. Consequently, T_{cs} degradation rate reduced from −106 mK to −5 mK per WUCD cycle after the sixth WUCD cycle, and after the ninth WUCD cycle, T_{cs} was nearly equal to 5.7 K.**

***Index Terms*—Cable-in-conduit conductor, current sharing temperature, ITER, niobium-tin.**

I. Introduction

THE ITER toroidal field (TF) coils are huge superconducting coils, 16.5 m in height and 9.2 m in width. The TF conductors are cable-in-conduit conductors (CICC) and are composed of a cable having 900 Nb_3Sn superconducting strands and 522 Cu strands, a central spiral tube, and a stainless-steel jacket, as shown in Fig. 1 [1]. The ITER TF coils will operate under a maximum magnetic field of 11.8 T and a current of 68 kA, and the TF conductors will be subjected to 1000 electromagnetic loading (EM) cycles over the lifetime of ITER. Therefore, the TF conductors are required to maintain a current sharing temperature (T_{cs}) greater than 5.7 K for 1000 electromagnetic loading (EM) cycles.

The National Institutes for Quantum Science and Technology (QST) procured 25% of the ITER TF conductors. Qualification tests were performed on the manufactured TF conductors at the SULTAN test facility [2], [3], [4], [5], [6]. In these tests at SULTAN, the T_{cs} of a straight, 3.6-m sample was measured under a current of 68 kA in a background field of 10.8 T, the results of which satisfied the ITER requirement of 5.7 K. However, these SULTAN tests cannot fully simulate the operating conditions of the ITER TF coils due to the large gradient of the magnetic field caused by the short length of the high field zone (450 mm), and the lack of hoop stress on the sample owing to its straight shape. To evaluate T_{cs} under a uniform field and with applied hoop stress, a solenoid TF insert coil (TFI) having a 40-m TF conductor was tested by using the CS model coil (CSMC) to apply a background field [7]. These TFI tests (performed in 2016–2017 and are referred to as the first test campaign), which simulated the operating conditions of the ITER TF coils, also showed that T_{cs} after 1000 EM cycles satisfied the ITER requirement (5.7 K). However, warm-up and cool-down (WUCD) cycles (including 6 quenches) of the TFI caused its T_{cs} to degrade, which raised concerns that T_{cs} might continue to decrease below 5.7 K before reaching 100 WUCD cycles (the designed value of ITER). From the results of this first TFI test campaign, it was not clear if T_{cs} would continue to degrade, thus, in 2018, a second TFI test campaign was carried out, during which four additional WUCD cycles were applied to the TFI and its T_{cs} was measured after each cycle. Moreover, to investigate the effects of EM cycles immediately after a WUCD cycle on T_{cs}, measurement, after each additional WUCD cycle, five EM cycles were performed, after which T_{cs} was measured again. This paper describes how the T_{cs} of the TFI was affected by WUCD cycles in the first and second test campaigns, conducted in 2016–2017 and 2018, respectively.

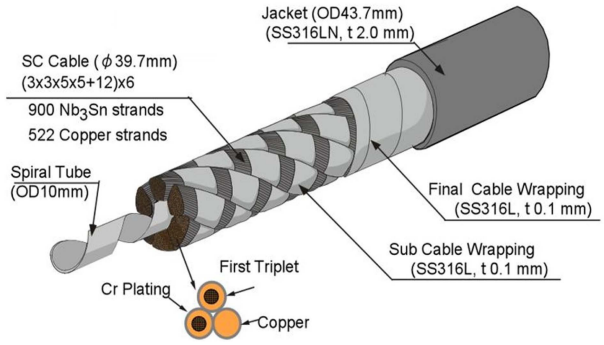

Fig. 1. Schematic of a TF conductor.

II. Experiment

A. TF Insert Coil and Instrumentation

The major specifications of the TF conductor and its Nb_3Sn strands used in the TFI are shown in Table I. The TFI is composed

Received 25 September 2024; revised 29 November 2024 and 10 December 2024; accepted 10 December 2024. Date of publication 13 December 2024; date of current version 31 December 2024. *(Corresponding author: Suwa Tomone.)*

The authors are with the National Institutes for Quantum Science and Technology, Naka 311-0193, Japan (e-mail: suwa.tomone@qst.go.jp).

Color versions of one or more figures in this article are available at https://doi.org/10.1109/TASC.2024.3517566.

Digital Object Identifier 10.1109/TASC.2024.3517566

TABLE I
SPECIFICATIONS OF THE TF CONDUCTOR AND NB3SN STRANDS FOR TFI

Item		Parameters
Nb_3Sn Strand	Type	Bronze route
	Diameter [mm]	0.822 mm
	Cu-non-Cu ratio	0.954
	RRR	147.6
	I_c(4.2 K, 12 T) [A]	229.5
Conductor	Cable layout	{(2Nb_3Sn+1Cu)×3×5×5+(3Cu×4)}×6
	Cable twist pitch [mm]	80×142×190×302×432
	Outer diameter [mm]	43.83
	Inner diameter [mm]	39.8
	Void fraction [%]	31.3

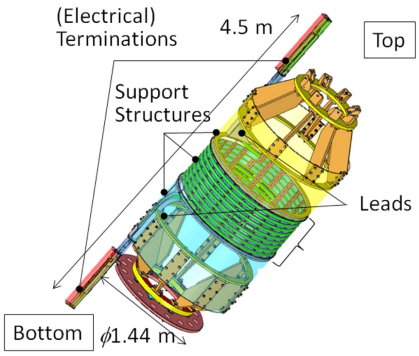

Fig. 2. Schematic of the TF insert coil (TFI).

of a solenoid TF conductor and a stainless-steel mandrel, as shown in Fig. 2. The 1.44-m-diameter solenoid was wound with the TF conductor, and a stainless steel mandrel was attached for support against the electromagnetic forces (simulated ITER TF coil operating conditions of 68 kA and 11.8 T). Vacuum pressure impregnation was later performed on the TFI for insulation and gap filling. The detailed fabrication process of the TFI is described in [8], [9]. To measure T_{cs}, the TFI was installed into the CSMC to apply a background field of 10.8 T [7], [10]. A sample for SULTAN was also fabricated by using the same conductor as that of the TFI and was heat treated simultaneously with the TFI conductor to compare differences between the TFI and SULTAN samples.

Voltage taps and thermometers (CERNOX) were installed in one turn of the TFI center, as shown in Fig. 3 [7], to measure the voltage and temperature for T_{cs} measurements. Four voltage taps (VD1011, VD1112, VD1213, VD1314), 1.1 m in length (1/4 turn), were placed on the conductor surface at the inner side of the TFI. There are also voltage taps called star taps, which are a set of six voltage taps located at a 60° angular distance on the surface of the conductor at the center of the TFI. Because the layout of the star taps is the same as that of the voltage taps of the SULTAN sample, the T_{cs} measured at the star tap can be directly compared with the T_{cs} measured by SULTAN. The thermometers were attached between voltage taps.

There are grooves on the mandrel at the location of a star tap and VD1112, as shown in Fig. 4. For the star tap, two 120-mm-long grooves were made to attach voltage taps on the conductor surface located between the mandrel and conductor.

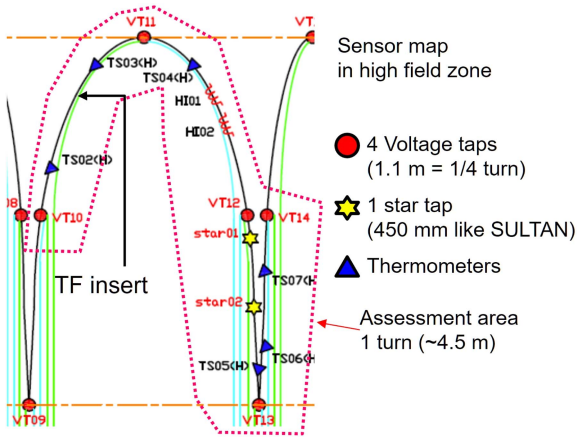

Fig. 3. Sensor map in one turn of TFI for T_{cs} assessment. The black line shows the TF conductor and the symbols show the sensors on the TFI.

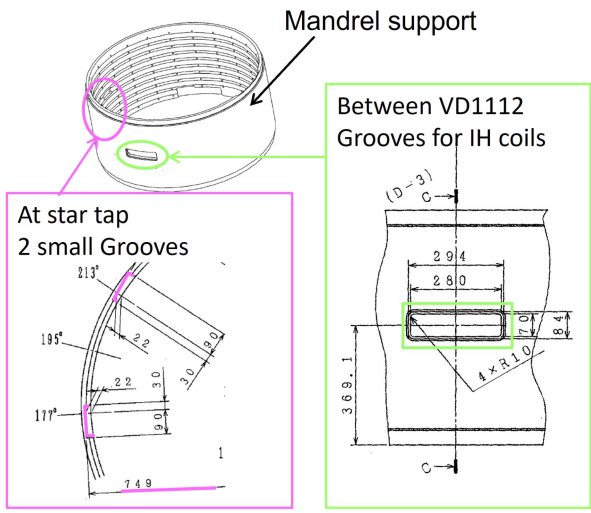

Fig. 4. Grooves on the mandrel at the star taps and VD1112.

For VD1112, there is a 280-mm groove to attach inductive heaters for quench tests. These grooves were filled with resin and glass cloth, but the conductor at these locations might be less supported against transverse electromagnetic forces than the other locations.

B. Assessment of T_{cs} and Effective Strain

T_{cs} was evaluated by measuring the voltage while holding the current and increasing the temperature of the conductor. The temperature of the conductor was increased by flowing He heated at the inlet of the TFI. T_{cs} was defined as the temperature at an electrical field of 10 μV/m. T_{cs} at the star tap was estimated as the average of T_{cs} evaluated by each voltage tap.

Since the critical current (I_c) of Nb_3Sn degrades by approximately 10% at a strain of 0.1%, [1], strain analysis was carried out by using effective strain to evaluate T_{cs} variation in the TFI test. The effective strain was calculated by using the curve fitting

TABLE II
PARAMETERS OF I_C (B, T, ε_{EFF}) FOR THE TFI

Parameters	Values
ε_m	0.00397
ε_{0a}	0.00231
C_{a1}	47.02
C_{a2}	11.76
B_{c2m}	32.35
T_{cm}	16.22
C_1	33000
p	0.84
q	2.57

(1) of the electrical field vs temperature curve,

$$E = \frac{E_c}{L_V A}\int_{L_V}\int_{A}\left(\frac{I_{op}}{N_{sc} I_c\,(B,T,\varepsilon_{eff})}\right)^n dA dz \qquad (1)$$

where E and T are measured electrical field and temperature, respectively. L_v is voltage tap length, A is the area of the cable in the conductor excluding the central spiral, I_{op} is the operating current, B is the magnetic field as a function of z, and N_{sc} is the number of Nb_3Sn strands. The fitting parameters are ε_{eff}, the effective strain, and n, the n value. $I_c\,(B,T,\varepsilon_{eff})$ is a representative strain-field-temperature dependence of I_c for Nb_3Sn strands [11]. The parameters of $I_c(B, T, \varepsilon_{eff})$ for the TFI are shown in Table II. However, ε_{eff} is an imaginary axial strain when only axial strain affects I_c (neglecting bending and transverse strain), and ε_{eff} is not perfectly equal to mechanical strain. For example, I_c degradation by bending and filament breakage moves ε_{eff} to the compressive side.

Moreover, measurement of T_{cs} and evaluation of ε_{eff} were performed in different electromagnetic force ($F_{EM} = I_{op} \times B$) conditions to investigate the influence of EM and WUCD cycles on the strain state of the conductor. It is considered that the F_{EM} vs ε_{eff} curve moves to the compressive side for ε_{eff} due to permanent I_c degradation by filament breakage and permanent strand bending or movement in the conductor. On the other hand, it is considered that a large negative F_{EM} dependence of ε_{eff} (absolute value is small) indicates that Nb_3Sn strands were easily deformed by F_{EM} due to an increase of gaps or an increase of distance between contact points (local twist pitch) by strands moving.

C. Test Campaigns for EM Cycles and WUCD Cycles

After finishing the first test campaign, the TFI and CSMC were warmed up to room temperature. To start the second test campaign, the TFI and CSMC were cooled down to about 4 K. This initial cool-down for the start of the second test campaign was counted as one WUCD cycle (sixth WUCD), after which only the TFI underwent three more WUCD cycles (from 4 K to 300 K) using the same procedure as the WUCD cycles of the first test campaign. Previous studies for SULTAN [6] and TFI [7] have shown a large decrease in T_{cs} with less than 50 EM cycles at the beginning of the tests. To investigate whether a similar large decrease in T_{cs} was induced by EM cycles immediately after a WUCD cycle, after each additional WUCD cycle and subsequent T_{cs} measurement (starting after the seventh WUCD cycle), five EM cycles were applied to the TFI, after which T_{cs} was measured again. The first and second test campaigns are summarized as follows:

-First test campaign
1) 1000 EM cycles.
2) First to third WUCD cycles.
3) Five quench tests.
4) Fourth to fifth WUCD cycles.
5) Margin test with quench.
6) Full warm-up of TFI and CSMC and one-year waiting period.

-Second test campaign
7) Cool-down of TFI and CSMC (counting as the sixth WUCD cycle).
8) Seventh to ninth WUCD cycles including 5 EM cycles after each WUCD cycle.

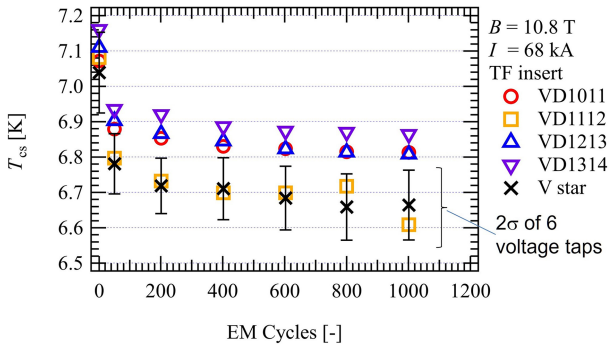

Fig. 5. Current sharing temperature (T_{cs}) against electromagnetic loading (EM) cycles.

III. RESULT

A. EM Cycles and T_{cs} Distribution in One Turn of TFI

Fig. 5 shows T_{cs} against EM cycles for the four voltage taps (VD1011, VD1112, VD1213, VD1314) and a star tap. The error bars for the star tap in Fig. 5 are 2σ of the T_{cs} calculated by the six voltage taps of the star tap; the T_{cs} of each individual voltage tap at the star tap are also within these error bars (±0.1 K). The T_{cs} of VD1112 was lower than those of the other voltage taps, which indicates that the T_{cs} might have been degraded by a larger strain caused by weak support of the conductor due to the large groove (shown in Fig. 4). For the star tap, the lower T_{cs} might have been caused by weak support of the conductor due to the two small grooves (shown in Fig. 4), and the deviation of the voltage around conductor surface because upper portion of the error bars is close to the T_{cs} of the other voltage taps. Therefore, T_{cs} at VD1112 is not appropriate for analysis, and T_{cs} assessment at the star tap would provide conservative results.

B. WUCD Cycles

As shown in Fig. 6(a), a linear T_{cs} degradation was observed in the WUCD cycles. The T_{cs} degradation rate ($\Delta T_{cs,WUCD}$) per WUCD cycle was calculated by linear fitting as shown in Table III. For this fitting, the current sharing temperature measurements after the fourth and fifth WUCD were excluded

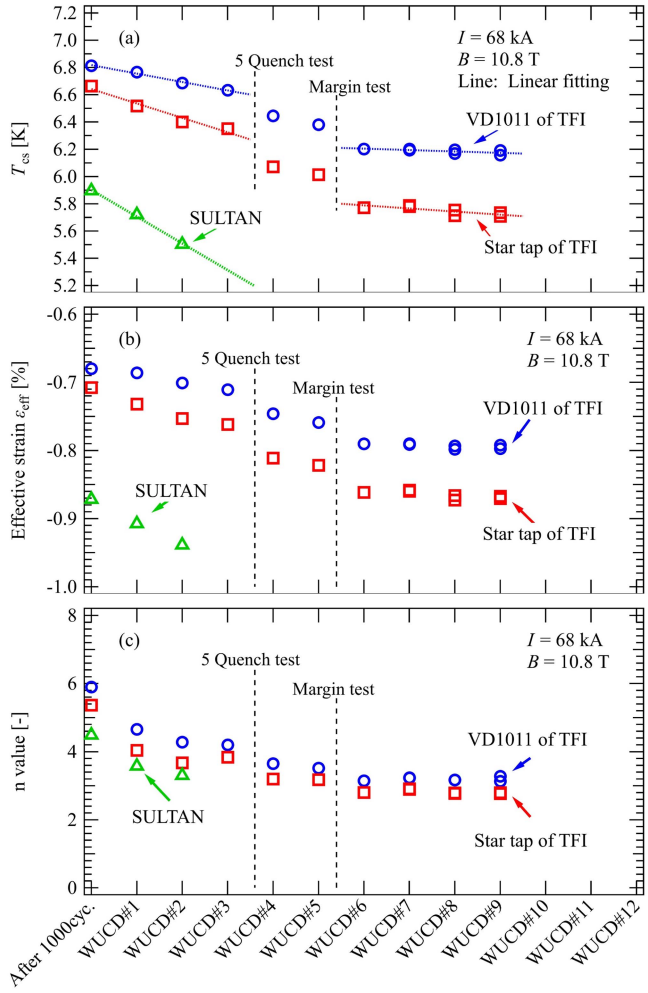

Fig. 6. T_{cs}, effective strain ε_{eff} and n value versus warm-up/cool-down (WUCD) cycles after 1000 EM cycles.

TABLE III
T_{cs} DEGRADATION PER WUCD CYCLE

Item	WUCD cycles	TFI		SULTAN
		Star tap	VD1011	
$\Delta T_{cs,WUCD}$ [mK/WUCD]	1st - 3rd	-106	-62	-196
	6th - 8th	-23	-11	-
	9th	-5	-12	

to evaluate degradation caused solely by WUCD cycles and not by quenches. Five quench tests were performed before the fourth WUCD, and the TFI quenched in the margin test before the fifth WUCD. Therefore, current sharing temperature measurements after the fourth and fifth WUCD cycles would include degradation by not only WUCD cycles but also quenches, which could cause local conductor temperature to increase to a maximum of 170 K [7]. Degradation of current sharing temperature caused by quenches was observed in the first test campaign [7]. The mechanism of T_{cs} degradation by quenches may be different from that of the WUCD cycles, because both local heating (thermal stress) and fast discharges [12] may degrade T_{cs} during a quench. To evaluate T_{cs} degradation caused solely by WUCD cycles, the effects of WUCD cycles and quenches should be

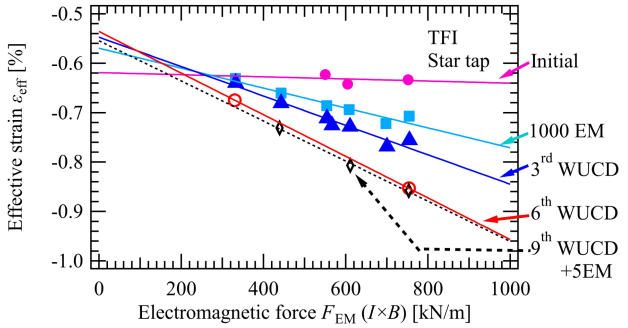

Fig. 7. Electromagnetic force (F_{EM}) dependence of ε_{eff} after EM cycles and WUCD cycles.

separated, however, this was not possible after the fourth and fifth WUCD cycles.

The T_{cs} degradation rate ($\Delta T_{cs,WUCD}$) of the TFI was less than half of that of the SULTAN tests. Between the sixth and eighth WUCD cycles, T_{cs} degradation continued, but $\Delta T_{cs,WUCD}$ reduced to approximately 10 mK per WUCD in the star tap. After the ninth WUCD cycle, $\Delta T_{cs,WUCD}$ was 5 mK, and degradation essentially stopped.

The ε_{eff} and n value are shown in Fig. 6(b) and (c), respectively. Both ε_{eff} and n value degraded until the sixth WUCD cycle, after which they both stabilized. Although degradation of ε_{eff} is not necessarily actual compressive strain variation in the axial direction caused by WUCD cycles, because I_c degradation of Nb_3Sn strands in the conductor due to the bending strain and filament breakage is evaluated as a decrease of ε_{eff} in (1).

C. Electromagnetic Force Dependence of Effective Strain

Variation of ε_{eff} caused by electromagnetic force (F_{EM}) was evaluated after EM cycles and WUCD cycles, as shown in Fig. 7. Based on these results, F_{EM} dependence of ε_{eff} were estimated. The lines in Fig. 7 were fitted by using the linear function $\varepsilon_{eff} = a_0 + a_1 F_{EM}$. A summary of the fitting parameters a_0 and a_1 are shown in Fig. 8. After the EM cycles and the sixth WUCD cycle, slope a_1 increased and the lines move to the compressive side, but this variation stabilized after the sixth WUCD cycle. Moreover, the additional five EM cycles starting after the seventh WUCD cycle did not degrade T_{cs} nor F_{EM} dependence of ε_{eff}.

IV. DISCUSSION

In a previous destructive examination of SULTAN samples, permanent deformation (e.g., bending) of Nb_3Sn strands was observed in the conductor after the SULTAN tests [13]. Moreover, fractured filaments were observed in the bent portions of the Nb_3Sn strands in the SULTAN samples [14], [15]. In the TFI, similar deformations and filament fractures may have been caused by electromagnetic forces and thermal stresses during the EM and WUCD cycles. As a consequence of these two permanent effects, I_c degradation and non-uniform distribution of I_c occurred in the conductor, causing T_{cs}, ε_{eff}, and n value to degrade after the EM and WUCD cycles. After the sixth WUCD cycle, these two irreversible effects might not be changed by the

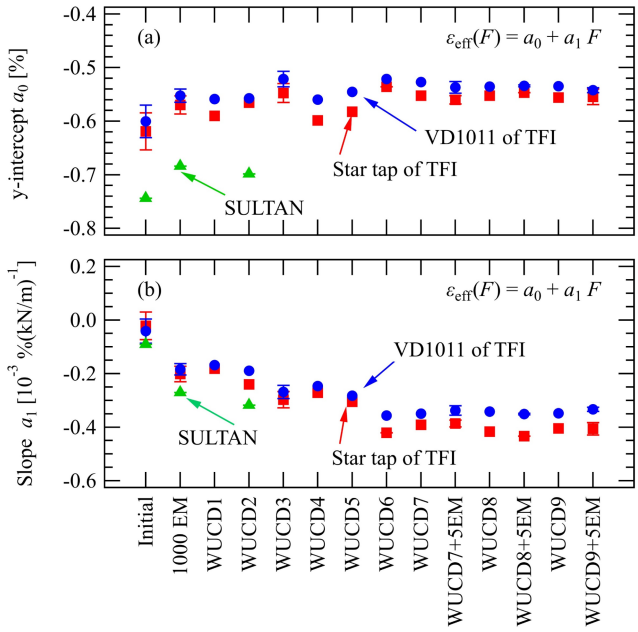

Fig. 8. Parameters of the linear fitting of ε_{eff} vs F_{EM}. Error bars show fitting error in cases having more than 3 data points.

additional WUCD cycles and subsequent five EM cycles, as no changes in T_{cs}, ε_{eff}, or n value were observed.

This permanent deformation can also be explained by the results of F_{EM} dependence of ε_{eff}. Permanent deformation (bent and displaced strands) caused by the EM and WUCD cycles may increase the gaps and distance between contact points of strands (i.e., local twist pitch) in the TFI. The larger the gaps, the larger the deflection that can be allowed on the strands in the conductor. Moreover, the longer the distance between contact points (longer local twist pitch), the larger the bending strain that can be induced by F_{EM}. Thus, Nb_3Sn strands in the TFI were easily deformed by a large F_{EM}, then the F_{EM} dependence has a larger negative value than that before applying the EM and WUCD cycles, as shown in Fig. 7.

In comparison with SULTAN, compressive ε_{eff} and the negative F_{EM} dependence are larger (absolute value is small) in the TFI. When hoop stress is applied to the strands in the TFI, tensile force exists in the axial direction of the strands. In case that the strand was bent, transverse component of this axial tensile force, which is opposite direction to the electromagnetic force, reduced the bending moment and bending strain.

V. Conclusion

T_{cs} degradation by warm-up and cool-down (WUCD) cycles was observed in the first test campaign (2016–2017), and there was concern that T_{cs} might continue to decrease to less than the ITER requirement of 5.7 K. To investigate the influence of WUCD cycles on T_{cs}, a second test campaign (2018) was performed, during which four additional WUCD cycles were applied to the TFI. As a result of both test campaigns for the TFI, T_{cs} degradation rate reduced from -106 mK to -5 mK per WUCD cycle after the ninth WUCD cycle, after which T_{cs} degradation stopped. After 1000 EM cycles and 9 WUCD cycles including 6 quenches, T_{cs} of the TFI satisfied the ITER requirement (5.7 K). Moreover, five EM cycles after the sixth WUCD cycle did not affect T_{cs}. However, T_{cs} degradation owing to quenches is not fully understood, and conductor performance might be degraded after a sixth quench in the actual operation of the ITER TF coils. The results of ε_{eff} analyses indicate permanent deformation and filament fracture on Nb_3Sn strands of the TFI were induced by the 1000 EM cycles and WUCD cycles until the 6th WUCD cycle. Furthermore, larger negative F_{EM} dependence of ε_{eff} than that of initial state also indicates that Nb_3Sn strands easily deformed by electromagnetic forces caused by an increase in the gaps and distance between contact points of the strands (local twist pitch) owing to permanent deformation of the strands.

Disclaimer

The views and opinions expressed herein do not necessarily reflect those of the ITER organization.

References

[1] A. Devred et al., "Challenges and status of ITER conductor production," *Supercond. Sci. Technol*, vol. 27, Mar. 2014, Art. no. 044001, doi: 10.1088/0953-2048/27/4/044001.

[2] J. W. Ekin, "Strain scaling law for flux pinning in practical superconductors. Part 1: Basic relationship and application to Nb_3Sn conductors," *Cryogenics*, vol. 20, pp. 611–624, Apr. 1980, doi: 10.1016/0011-2275(80)90191-5.

[3] P. Bruzzone et al., "Test of ITER conductors in SULTAN: An update," *Fus. Eng. Des*, vol. 86, pp. 1406–1409, Oct. 2011, doi: 10.1016/j.fusengdes.2011.02.061.

[4] Y. Takahashi et al., "Performance of Japanese Nb_3Sn conductors for ITER toroidal field coils," *IEEE Trans. Appl. Supercond.*, vol. 18, no. 2, pp. 471–474, Jun. 2008, doi: 10.1109/TASC.2008.921866.

[5] K. Matsui et al., "Test results of third Japanese SULTAN sample," *IEEE Trans. Appl. Supercond.*, vol. 19, no. 3, pp. 1470–1473, Jun. 2009, doi: 10.1109/TASC.2009.2017696.

[6] M. Bresci et al., "Performance analysis of the toroidal field ITER production conductors," *Supercond. Sci. Technol*, vol. 30, Apr. 2017, Art. no. 055007, doi: 10.1088/1361-6668/aa6785.

[7] H. Ozeki et al., "T_{cs} measurement result of ITER toroidal field insert coil tested in 2016," *IEEE Trans. Appl. Supercond.*, vol. 28, no. 3, Apr. 2018, Art. no. 4202905, doi: 10.1109/TASC.2017.2787656.

[8] H. Ozeki et al., "Fabrication process qualification of TF insert coil using real ITER TF conductor," *IEEE Trans. Appl. Supercond.*, vol. 25, no. 3, Jun. 2015, Art. no. 4200804, doi: 10.1109/TASC.2014.2364393.

[9] H. Ozeki et al., "Manufacture and quality control of insert coil with real ITER TF conductor," *IEEE Trans. Appl. Supercond.*, vol. 26, no. 4, Jun. 2016, Art. no. 4202504, doi: 10.1109/TASC.2016.2537150.

[10] T. Ando et al., "ITER central solenoid (CS) model coil project," *TEION KOGAKU (J. Cryogenics Supercond. Soc. Jpn)*, vol. 36, no. 6, pp. 309–314, Jun. 2001, doi: 10.2221/jcsj.36.309.

[11] L. Bottura et al., "J_c (B, T, ε;) parameterization for the ITER Nb_3Sn production," *IEEE Trans. Appl. Supercond.*, vol. 19, no. 3, pp. 1521–1524, Jun. 2009, doi: 10.1109/TASC.2009.2018278.

[12] K. Sedlak et al., "T_{cs} degradation of ITER TF samples due to fast current discharges," *Supercond. Sci. Technol*, vol. 34, Jan. 2021, Art. no. 025004, doi: 10.1088/1361-6668/abc8cd.

[13] Y. Nabara et al., "Examination of Japanese mass-produced Nb_3Sn conductors for ITER toroidal field coils," *IEEE Trans. Appl. Supercond.*, vol. 22, no. 3, Sep. 2011, Art. no. 4804804, doi: 10.1109/TASC.2011.2178990.

[14] C. Sanabria et al., "Metallographic autopsies of full-scale ITER prototype cable-in-conduit conductors after full testing in SULTAN: 1. The mechanical role of copper strands in a CICC," *Supercond. Sci. Technol*, vol. 28, Jun. 2015, Art. no. 085005, doi: 10.1088/0953-2048/28/8/085005.

[15] N. Mitchell et al., "The use of Nb_3Sn in fusion: Lessons learned from the ITER production including options for management of performance degradation," *Supercond. Sci. Technol*, vol. 33, Mar. 2020, Art. no. 054007, doi: 10.1088/1361-6668/ab7ec2.